Proceedings of ASME 2007 International Design Engineering Technical Conferences & Computers and Information in Engineering Conference
IDETC/CIE 2007
September 4-7, 2007, Las Vegas, NV, USA

DETC2007-35777

STRUCTURAL DESIGN TRADE-OFFS FOR MEMS VIBRATORY RATE GYROSCOPES WITH 2-DOF SENSE MODES

Adam R. Schofield * **Alexander A. Trusov** **Andrei M. Shkel**

MicroSystems Laboratory
Department of Mechanical and Aerospace Engineering
University of California, Irvine
Irvine, CA 92697

ABSTRACT

Our previous work demonstrated the advantages of MEMS vibratory gyroscopes with 1 degree of freedom (DOF) drive and 2-DOF sense modes which were shown to be robust to temperature drifts. These devices were designed with frequencies below 1 kHz; many applications, however, require gyroscopes with operational frequencies above 1 kHz for the rejection of ambient vibrations. This paper discusses the design trade-offs associated with increasing the frequency of the 3-DOF gyroscope design concept. Lumped parameter models were used to simulate the effects of frequency increases on the device, focusing on the 2-DOF sense mode. The simulations showed that the sense mode peak spacing increases with frequency which ultimately causes a decrease in sensitivity. A series of 3-DOF gyroscope prototypes with different operational frequencies ranging from 0.7 kHz to 5.1 kHz were designed, fabricated, and characterized.

INTRODUCTION

All vibratory micromachined gyroscopes integrate two high precision subsystems – a self tuned oscillator, called the drive mode, and a micro-g accelerometer, called the sense mode [1, 2]. The operation of the device depends on a transfer of energy between these modes which is detected and processed to produce the device output [1]. While these subsystems are generally designed to have their own independent vibration characteristics, the complete sensor dynamics are sensitive to the relative location of the drive and sense resonant frequencies [3].

Conventional micromachined vibratory gyroscopes generally use a single degree of freedom for both the drive and sense mode, forming a 2-DOF dynamic system [2, 3]. For these types of devices, the sensor gain can be increased by mode matching, where the drive and sense natural frequencies are designed to be equal. The increased gain comes at the cost of robustness as fluctuations in the operational parameters can cause large changes in amplitude due to the instability of resonance [3]. Because of this, conventional devices are generally designed with a few percent mismatch in frequencies.

The 3-DOF micromachined gyroscope is a novel design concept introduced in [4]. The difference of this design from conventional devices is the addition of a second sense mass, forming a coupled 2-DOF sense mode. This alters the frequency response so that a region of magnitude and phase stability is formed between the two coupled resonant frequencies. Using low frequency prototypes, it was demonstrated that this design approach yields angular rate sensors robust to fabrication imperfections and environmental conditions [4]. However, the 3-DOF design approach has been shown to have drawbacks associated with increases in operational frequencies, where increases in peak spacings can cause a drop in sensor gain [5].

This paper investigates the effects of increasing the oper-

*Author of correspondence, Email: adam.schofield@uci.edu

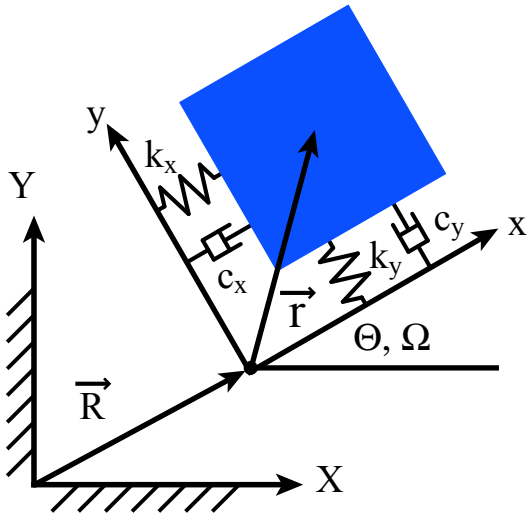

Figure 1. SCHEMATIC DEPICTING A MASS SUSPENDED IN A ROTATING COORDINATE FRAME

ational frequency of MEMS vibratory gyroscopes with 2-DOF sense modes. Modeling results of the trade-offs associated with these increases are presented here. In order to show the feasibility of increased frequency 3-DOF gyroscopes, a redesign of the device with a smaller mass ratio was fabricated and characterized. Rate response characterizations of micromachined 3-DOF gyroscopes with various operational frequencies are presented.

GYROSCOPE DYNAMICS

Vibratory rate gyroscopes take advantage of the Coriolis effect, where a moving object in a rotating coordinate system experiences rotation induced accelerations perpendicular to both the rotation and its motion. For micromachined implementations, this is typically a suspended proof mass that is free to move in two directions, as shown schematically in Fig. 1. If the position of this mass is defined relative to a coordinate frame attached to its anchors and this coordinate frame is rotating, the acceleration of the mass can be expressed in vector form as

$$\vec{A} = \ddot{\vec{R}} + \ddot{\vec{r}} + \dot{\vec{\Omega}} \times \vec{r} + \vec{\Omega} \times \left(\vec{\Omega} \times \vec{r}\right) + 2\vec{\Omega} \times \dot{\vec{r}} \qquad (1)$$

where $\ddot{\vec{R}}$ is the acceleration of the coordinate frame $\{x,y\}$ relative to an inertial frame $\{X,Y\}$, $\ddot{\vec{r}}$ is the acceleration of the mass in the rotating frame $\{x,y\}$, and $\vec{\Omega}$ is its angular velocity vector. Since most gyroscopes are typically designed to be sensitive to a single axis of rotation, it is assumed that $\vec{\Omega}$ contains only one non-zero component of rotation, Ω_z, corresponding to in-plane rotations. Equation (1) can now be simplified to the following

$$A_x = \ddot{X} + \ddot{x} - \dot{\Omega}_z y - \Omega_z^2 x - 2\Omega_z \dot{y} \qquad (2)$$
$$A_y = \ddot{Y} + \ddot{y} + \dot{\Omega}_z x - \Omega_z^2 y + 2\Omega_z \dot{x} \qquad (3)$$

where $\ddot{X}$ and $\ddot{Y}$ represent the acceleration of the moving coordinate system $\{x,y\}$ with respect to the inertial frame $\{X,Y\}$, $\ddot{x}$ and $\ddot{y}$ represent the acceleration of the mass with respect to the moving frame $\{x,y\}$, $\dot{\Omega}_z y$ and $\dot{\Omega}_z x$ are the angular acceleration terms, $\Omega_z^2 x$ and $\Omega_z^2 y$ are the centrifugal acceleration terms, and $\Omega_z \dot{y}$ and $\Omega_z \dot{x}$ are the Coriolis acceleration terms.

The Coriolis terms in Eqn. (2) and (3) cause a transfer of energy from x to y (and consequently from y to x) proportional to the angular rate while the other terms act to corrupt this information. Vibratory gyroscopes, however, are often used to measure a small range of rotations, typically $\pm$ 300 deg/sec, therefore, the angular acceleration terms proportional to Ω_z^2 are generally small compared to device frequencies and can be neglected. If the sensor is restricted to measure constant or near constant angular rates, the centrifugal terms proportional to $\dot{\Omega}_z$ can also be neglected.

Using the model in Fig. 1 and the accelerations in Eqn. (2) and (3) without the neglected terms, the equations of motion for the mass can be expressed as

$$M\ddot{x} + c_x\dot{x} + k_x x = F_x - Ma_x + 2M\Omega_z\dot{y} \qquad (4)$$
$$M\ddot{y} + c_y\dot{y} + k_y y = F_y - Ma_y - 2M\Omega_z\dot{x} \qquad (5)$$

where a_x and a_y are any external accelerations while F_x and F_y are any external forces applied to the mass. Even though the effect of acceleration loads on vibratory gyroscopes is a topic of interest, it is beyond the scope of this paper. Therefore the acceleration terms are assumed to be compensated by signal processing and will be neglected.

Equation (4) and (5) define the dynamic system that is the basis for vibratory rate gyroscopes. The next sections will expand these equations for both conventional and 3-DOF implementations.

Conventional Implementation

Conventional vibratory rate gyroscopes consist of a single degree of freedom drive and sense mode, much like the system defined by Eqn. (4) and (5). Most micromachined implementations, however, utilize mechanical mode decoupling between drive and sense. This is accomplished by suspending a sense mass inside of a decoupling frame as shown in Fig. 2. The decoupling frame is constrained so that it only oscillates in the drive direction, while the sense mass is suspended so that it moves only in the sense direction relative to the frame. The dynamic system

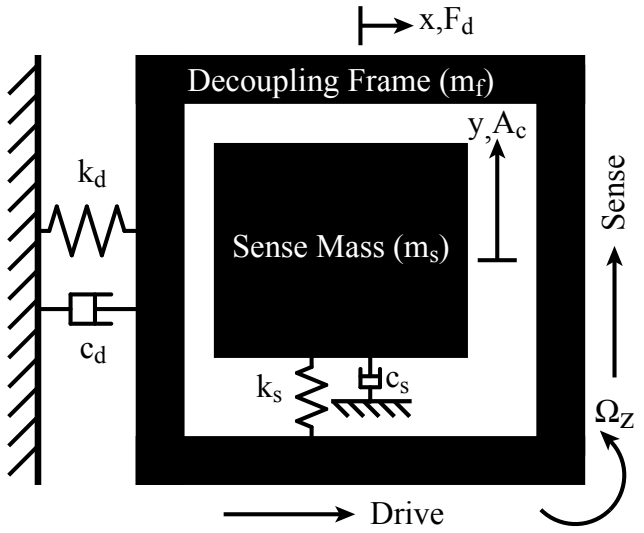

Figure 2. LUMPED PARAMETER MODEL OF A CONVENTIONAL GYROSCOPE WITH MECHANICAL MODE DECOUPLING

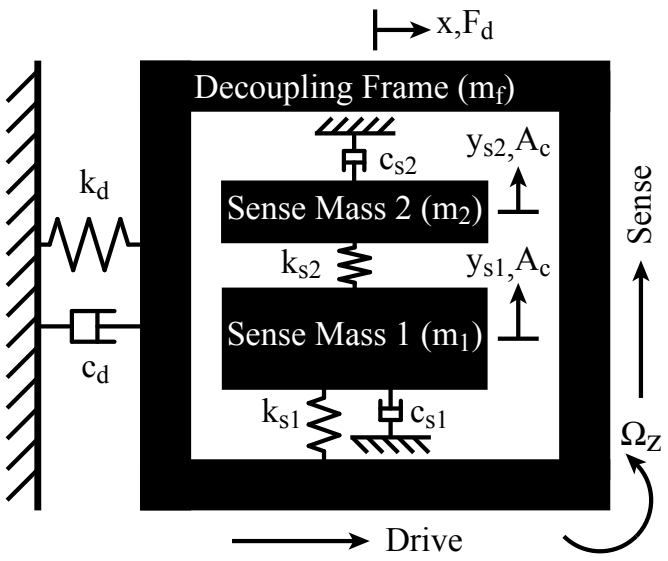

Figure 3. LUMPED PARAMETER MODEL OF A 3-DOF GYROSCOPE WITH MECHANICAL MODE DECOUPLING

can then be represented by the following equations:

$$(m_f + m_s)\ddot{x} + c_d\dot{x} + k_d x = F_d \tag{6}$$

$$m_s\ddot{y} + c_s\dot{y} + k_s y = -2m_s\Omega_z\dot{x} \tag{7}$$

where the drive direction is assumed to be along the x axis, the sense direction is along the y axis, m_f is the mass of the decoupling frame, m_s is the mass of the sense mass, c_d is the total damping coefficient between both masses and the substrate along the drive direction, c_s is the total damping coefficient between the sense mass and the substrate in the sense direction, k_d is the drive mode stiffness, k_s is the sense mode stiffness, F_d is the applied driving force, and Ω_z is the angular rate.

The drive mode is represented by Eqn. (6) and consists of both the decoupling frame and sense mass moving together in the drive direction due to a forcing input on the frame. The natural frequency of this mode is determined by the total mass, $M_d = m_f + m_s$, and the decoupling frame stiffness, k_d. The Coriolis term has been neglected by assuming there is an active control for keeping the drive mode amplitude constant. The sense mode response is represented by Eqn. (7). It also has a single degree of freedom and its natural frequency is determined by the sense mass, m_s, and the sense mode stiffness, k_s. It is only forced into vibration when the system is subject to an input angular rate, Ω_z.

3-DOF Implementation

The mechanical structure of the 3-DOF gyroscope consists of a single degree of freedom drive mode and a 2-DOF sense mode. It also uses mechanical mode decoupling where the two sense masses are suspended inside of a decoupling frame as shown in Fig. 3. The decoupling frame is constrained so that it only oscillates in the drive direction while the sense masses are constrained to vibrate only in the sense direction relative to the frame. Thus, the ideal system can be represented by the following simplified equations:

$$(m_f + m_1 + m_2)\ddot{x} + c_d\dot{x} + k_d x = F_d \tag{8}$$

$$m_1\ddot{y}_1 + c_1\dot{y}_1 + (k_1 + k_2)y_1 - k_2 y_2 = -2\dot{x}m_1\Omega_z \tag{9}$$

$$m_2\ddot{y}_2 + c_2\dot{y}_2 + k_2 y_2 - k_2 y_1 = -2\dot{x}m_2\Omega_z \tag{10}$$

where the drive direction is assumed to be along the x axis, the sense direction is along the y axis, m_f is the mass of the decoupling frame, m_1 is the mass of sense mass 1, m_2 is the mass of sense mass 2, c_d is the total damping coefficient between all masses and the substrate along the drive direction, c_1 is the total damping coefficient between sense mass 1 and the substrate in the sense direction, c_2 is the total damping coefficient between sense mass 2 and the substrate in the sense direction, k_d is the drive mode stiffness, k_1 is the stiffness between the frame and sense mass 1, k_2 is the stiffness between sense mass 1 and sense mass 2, F_d is the applied driving force, and Ω_z is the angular rate.

The drive mode is represented by Eqn. (8) which consists of the decoupling frame and both sense masses moving in unison in the drive direction due to a harmonic forcing applied to the frame. This is identical to the conventional drive mode defined in Eqn. (6) with the exception of the additional sense mass. The

sense mode dynamics are represented by Eqn. (9) and (10) in terms of the displacements of both sense masses, y_1 and y_2, in the sense direction. They form a 2-DOF coupled system where both masses are forced into vibration when subject to an input angular rate.

Since the drive mode is a conventional resonator, the focus will now shift to the 2-DOF sense system defined by Eqn. (9) and (10). In order to determine the resonant frequencies of the coupled system in terms of the model parameters, the following quantities are defined:

$$\omega_1^2 = \frac{k_1+k_2}{m_1} \tag{11}$$

$$\omega_2^2 = \frac{k_2}{m_2} \tag{12}$$

$$\mu^2 = \frac{m_2}{m_1} \tag{13}$$

where Eqn. (11) corresponds to the uncoupled natural frequency of sense mass 1, Eqn. (12) corresponds to the uncoupled natural frequency of sense mass 2, and Eqn. (13) defines the mass ratio. Substituting these expressions in Eqn. (9) and (10) yields the following representation of the sense mode dynamics:

$$\ddot{y}_1 + \frac{c_1}{m_1}\dot{y}_1 + \omega_1^2 y_1 - \mu^2\omega_2^2 y_2 = -2\dot{x}\Omega_z \tag{14}$$

$$\ddot{y}_2 + \frac{c_2}{m_2}\dot{y}_2 + \omega_2^2 y_2 - \omega_2^2 y_1 = -2\dot{x}\Omega_z \tag{15}$$

Since this is a coupled system, the natural frequencies defined in Eqn. (11) and (12) do not correspond to the actual resonant frequencies that would be seen in the frequency response. From a design point of view, it is easier to start with the sense mode peak locations, ω_{c1} and ω_{c2}, which can then be used to determine the layout parameters needed to achieve the desired system. Using Eqn. (14) and (15), the following equations can be found,

$$\omega_1^2 = \frac{\omega_{c2}^2}{2} + \frac{\omega_{c1}^2}{2} + \sqrt{\left(\frac{\omega_{c2}^2}{2} - \frac{\omega_{c1}^2}{2}\right)^2 - \mu^2\omega_2^4} \tag{16}$$

$$\omega_2^2 = \frac{\omega_{c2}^2}{2} + \frac{\omega_{c1}^2}{2} - \sqrt{\left(\frac{\omega_{c2}^2}{2} - \frac{\omega_{c1}^2}{2}\right)^2 - \mu^2\omega_2^4} \tag{17}$$

which defines the relationship between the uncoupled natural frequencies, ω_1, ω_2, the actual sense mode resonant peaks ω_{c1}, ω_{c2}, and mass ratio, μ^2. When solving Eqn. (17) for the uncoupled natural frequency ω_2^2, a condition on the mass ratio is revealed in order to have a valid physical system. This condition is given by

$$\mu^2 < \mu_c^2 = \frac{\omega_{c2}^4 - 2\omega_{c2}^2\omega_{c1}^2 + \omega_{c1}^4}{4\omega_{c2}^2\omega_{c1}^2} \tag{18}$$

where ω_{c1}, ω_{c2} are the desired sense mode resonant frequencies and μ_c^2 is the critical mass ratio. Thus, given any two desired peak locations, the maximum mass ratio required to achieve this design can be determined from Eqn. (18). A system with a mass ratio lower than the critical mass ratio for a given peak spacing is physically achievable while designing a system for this peak spacing with a larger mass ratio is impossible.

Design Comparison

The difference between a conventional and a 3-DOF approach can be seen by examining the typical frequency responses of both systems. Figure 4(a) conceptually shows the magnitude plot of a mode mismatched conventional gyroscope. As expected, there are two resonant peaks corresponding to the two 1-DOF systems.

Figure 4(b) conceptually shows the magnitude plot of a 3-DOF gyroscope. There are three curves corresponding to the drive mode and both sense masses. The single DOF drive mode results in a single resonance peak, while the coupling of the two masses in the sense mode results in two resonant frequencies, and thus two peaks in the frequency response. This coupling also creates a region of relatively constant gain between the peaks for the smaller sense mass 2. By designing the drive mode resonant frequency to be in this region and detecting the Coriolis signal from the smaller sense mass, m_2, one takes advantage of the non-resonant sense mode amplitude which is stable in both magnitude and phase over a wide frequency range.

This flat region in the frequency response provides the 3-DOF gyroscope with improved robustness by design. Fabrication imperfections and environmental changes can cause shifts in the desired resonant frequencies of the device. For conventional devices, a mismatch between the drive and sense resonant frequencies helps to improve robustness by moving away from the sense mode resonance to a more stable location in the frequency response, but it comes at the cost of lower sensitivity due to the reduction in amplitude [3]. The constant gain region between the peaks of the 3-DOF gyroscope accomplishes the same goal of non-resonant stability, however the reduction in amplitude can be minimized by controlling the sense mode peak spacing.

SIMULATION RESULTS

1-DOF Sense Mode

The conventional sense mode equation of motion given by Eqn. (7) was simulated to determine the effects of increasing the operational frequency on the system. Figure 5 shows the frequency response for three different sense mode natural frequencies for constant forcing, mass, and damping coefficients. As the natural frequency is increased, the overall amplitude drops resulting in nearly two orders of magnitude difference from 700 Hz to 5.1 kHz. This can be attributed to the increases in stiffness

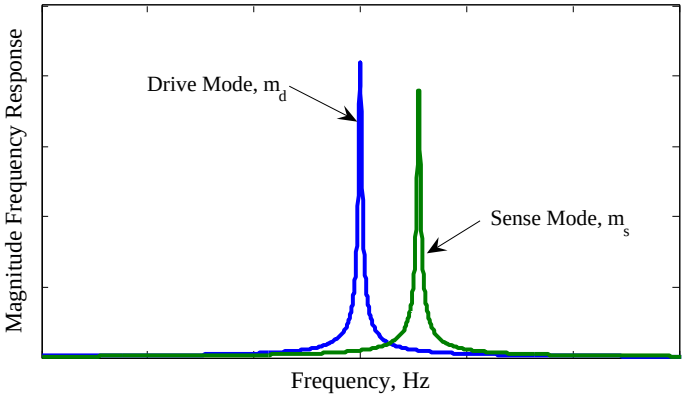

(a) CONVENTIONAL

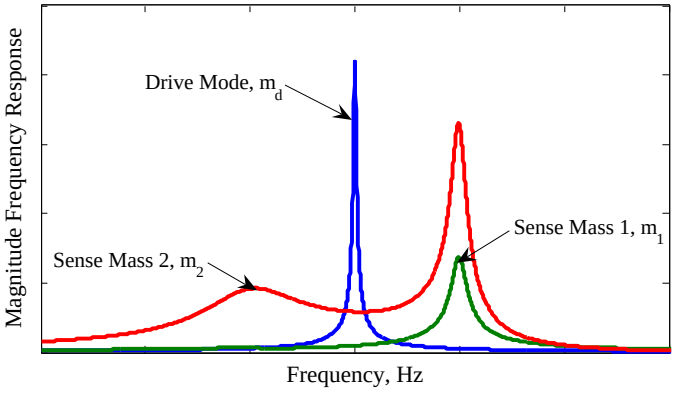

(b) 3-DOF

Figure 4. TYPICAL FREQUENCY RESPONSE PLOTS FOR A CONVENTIONAL MODE MISMATCHED AND 3-DOF GYROSCOPE

required for the larger frequencies and will also be observed in 2-DOF sense systems.

2-DOF Sense Mode

The 2-DOF sense mode given in Eqn. (14) and (15) was examined to determine how increasing the operational frequency affects the dynamic system. Figure 6 shows the magnitude of the frequency response at three different frequencies for constant forcing, mass ratio, and damping coefficients. Much like the conventional sense mode, increasing the frequency results in an overall drop in amplitude. A more interesting result is that the peak spacing also increases with frequency which results in a decrease of the sense mode amplitude in the operating region between the peaks. This is a direct result of Eqn. (18), where increases in ω_1 for constant mass ratios result in larger ω_2 values.

The observed drop in sense mode amplitude between the peaks has a direct effect on the sensor output. Figure 7 shows simulated rate response plots for the three operational frequencies with increasing peak spacings. As the peak spacings get

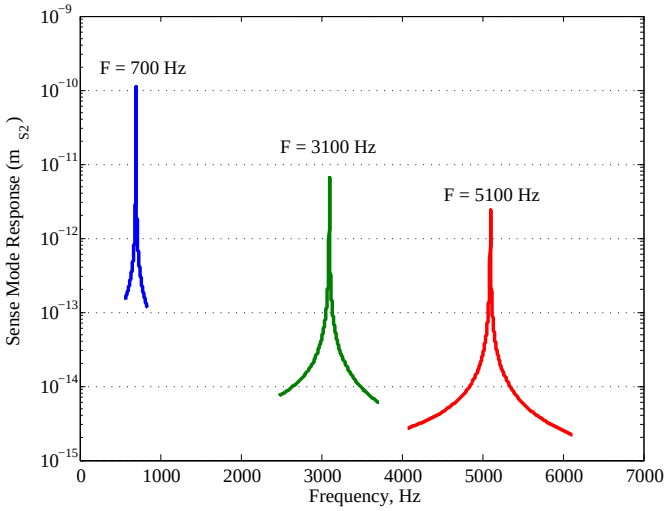

Figure 5. CONVENTIONAL SENSE MODE FREQUENCY RESPONSES FOR VARIOUS OPERATIONAL FREQUENCIES

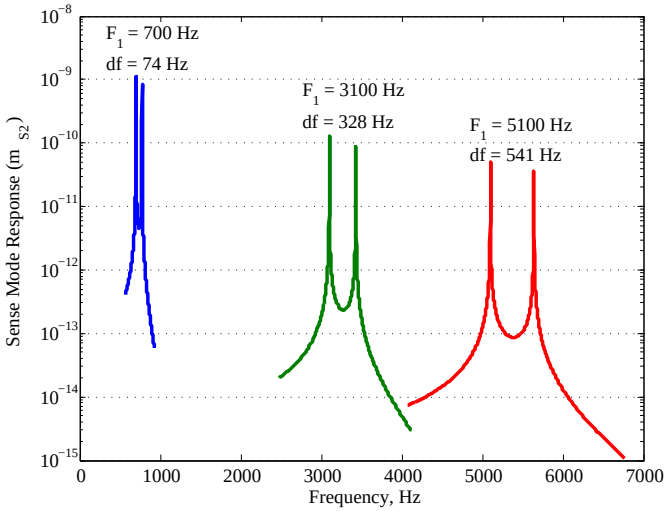

Figure 6. 3-DOF SENSE MODE FREQUENCY RESPONSE PLOTS AS A FUNCTION OF OPERATIONAL FREQUENCY

larger for constant forcing, the sensitivity decreases. In order to restore the sensitivity, larger actuation voltages are required which results in increased noise.

One way to alleviate the increase in peak spacing for increasing frequencies is to not only adjust stiffnesses, but also lower the mass ratio. Figure 8 plots the critical mass ratio versus frequency for various peak spacings. For high frequencies and small spacings, the mass ratios needed correspond to at least 3-4 orders of magnitude difference in mass. This requires systems with a much larger sense mass 1 than smaller sense mass 2, meaning ei-

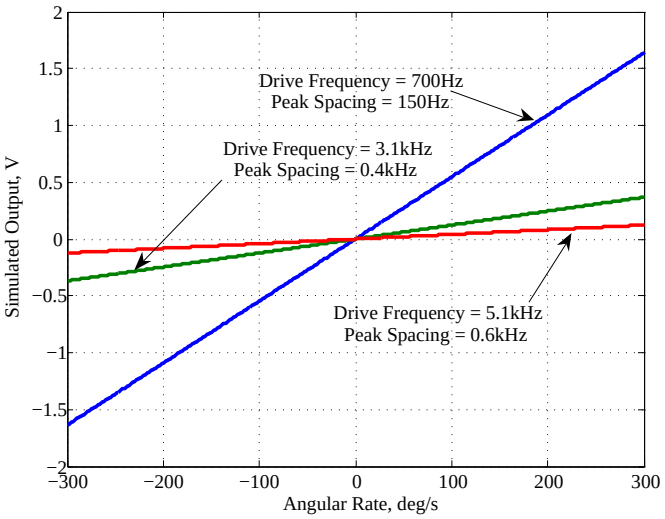

Figure 7. SIMULATED RATE RESPONSE PLOT FOR DIFFERENT OPERATIONAL FREQUENCIES AND SENSE MODE PEAK SPACINGS

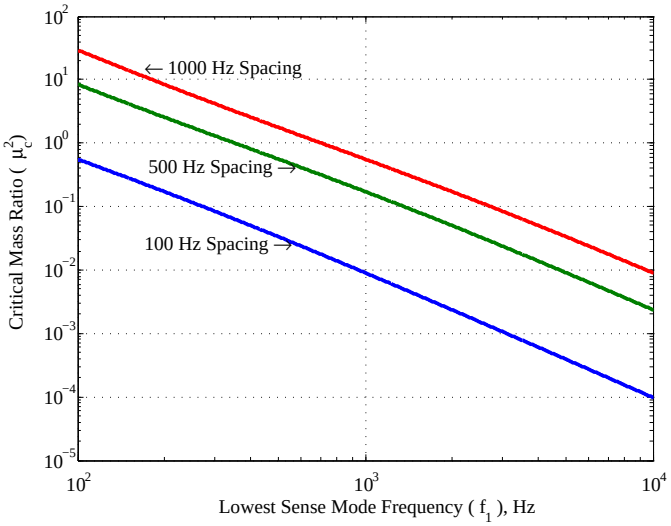

Figure 8. CRITICAL MASS RATIO FOR INCREASING FREQUENCY FOR VARIOUS PEAK SPACINGS

ther very large device sizes or fewer Coriolis sensing capacitors.

EXPERIMENTAL RESULTS

Fabrication

Several 3-DOF devices were designed, fabricated, and characterized. The fabrication was done using a wafer level SOI process. SOI wafers with a conductive 75 μm thick device layer were used. Shipley 1827 photo-resist was spin-coated onto the

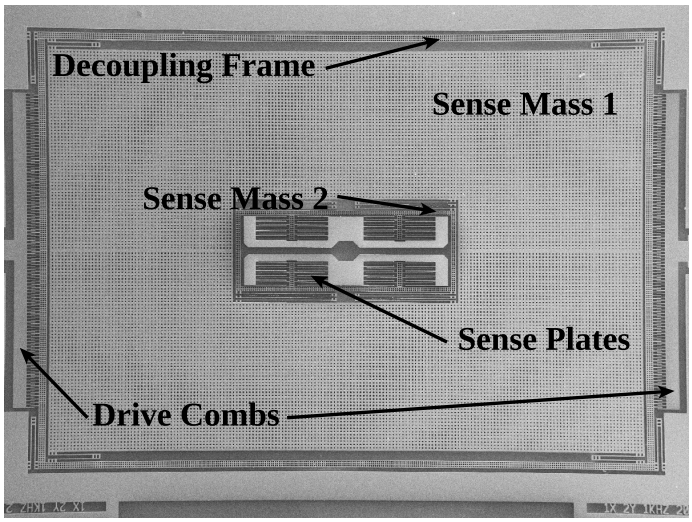

Figure 9. SEM IMAGE OF A FABRICATED 3-DOF GYROSCOPE PROTOTYPE

wafers and patterned using a chrome-on-glass photo-mask and a Karl Suss MA6 exposure system. After photo-resist development, the wafers were subjected to a timed Deep Reactive Ion Etching (DRIE) using a Surface Technology Systems (STS) tool. The minimum feature of the process was 8 μm. Figure 9 shows an SEM image of a fabricated 3-DOF gyroscope. The drive mode decoupling frame utilizes lateral comb drive capacitors and the motion of the smaller sense mass is detected using parallel plate capacitors.

Experimental Setup

Figure 10 shows a schematic of the actuation and detection scheme used to characterize the gyroscopes. A combination of a DC bias with a driving AC voltage is applied to the fixed driving electrode; vibration of the drive mode decoupling frame is excited at the frequency of the driving AC voltage. The driving AC voltage also causes a flow of parasitic current that contributes to the total pick-up current used for motion detection. Electromechanical Amplitude Modulation (EAM) was used to detect the motion of the sense mass. EAM uses a carrier AC voltage across the sense capacitor, which results in the Amplitude Modulation (AM) of the variable sense capacitance. This elevates the motional signal away from parasitic feed-through of the drive voltage [6]. Two stage demodulation was used to extract the motional signal from the total EAM pick-up signal. Each demodulation block consists of a reference harmonic phase shift, mixing, and band-pass filtering.

For this work, two AMETEK Advanced Measurement Technology Signal Recovery Model 7265 digital lock-in amplifiers were used to generate the drive and the carrier AC voltages and perform the two stages of demodulation. An HP 35665A Dy-

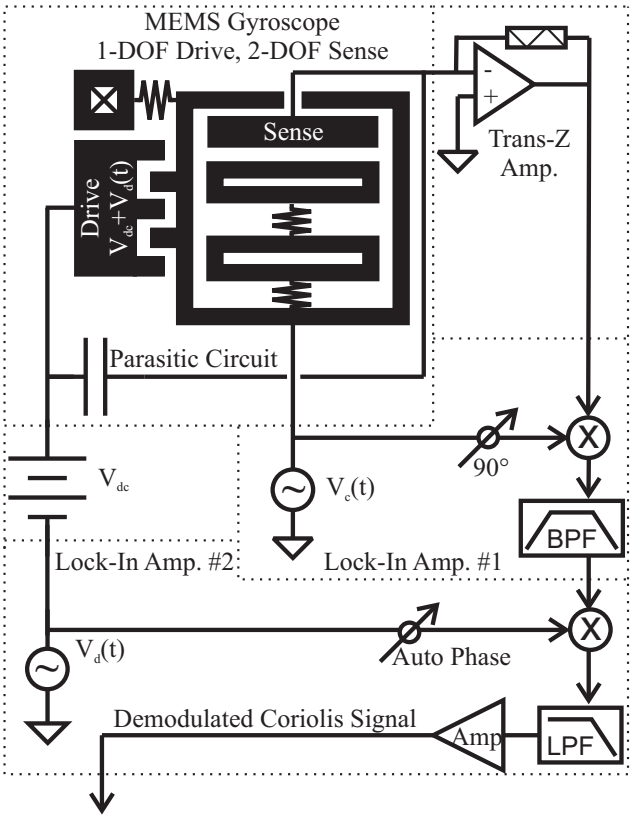

Figure 10. BIASING SCHEMATIC USING OPEN LOOP ACTUATION AND EAM BASED CORIOLIS DETECTION

namic Signal Analyzer was used to collect two data channels – the demodulated output of the gyroscope, and the angular rate reference signal produced by the rate table. For simplicity, in all described experiments the detection was done using a single sensing capacitor.

Constant Angular Rate Characterization

Several MEMS implementations of the 3-DOF concept were tested: a low frequency 700 Hz device with 150 Hz sense mode spacing, a 3.1 kHz device with sense mode resonant frequency spacing of 0.4 kHz, and a 5.1 kHz device with a 0.6 kHz sense spacing. The steady state responses of the gyroscopes were collected for different values of the input angular rate. Figure 11 shows the rate response of a gyroscope with 700 Hz drive mode resonant frequency and 150 Hz sense mode spacing. The device shows RMS nonlinearity error of 0.084 % full scale output (FSO) in the $\pm$1000 deg/s range. This device has the same operational frequency as the one previously reported in [4], however, it is redesigned for a 5 times smaller sense mode mass ratio in order for frequency scaling with closer peak spacing. Figure 12 shows the response of the 3-DOF gyroscope with 3.1 kHz drive mode

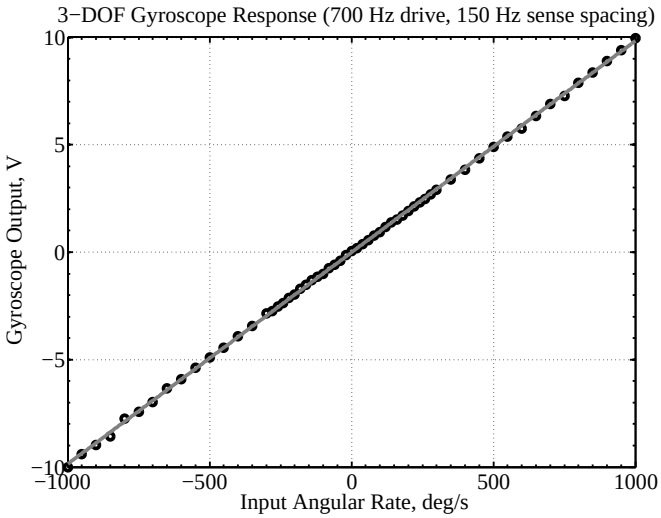

Figure 11. LOWER FREQUENCY 3-DOF GYROSCOPE RESPONSE (700 HZ DRIVE, 150 HZ PEAK SPACING)

resonant frequency and 0.4 kHz spacing between the sense mode resonant frequencies. For this device, the nonlinearity error is 0.38% FSO in the $\pm$1000 deg/s. The response of the 3-DOF device with 5.1 kHz drive mode resonant frequency and 0.6 kHz sense mode spacing is shown in Fig. 13. This device has a nonlinearity error of 0.76% FSO in the $\pm$1000 deg/s range.

The operational frequency of the devices presented here were scaled 4 and 7 times that of the device originally reported in [4]. An analysis of the measured nonlinearity errors shows that the performance of 3-DOF gyroscopes degraded proportionally to the increase of the operational frequency. Drops in the mechanical sensitivity of the 2-DOF sense mode and a decrease of the signal-to-noise ratio caused by larger actuation voltages both contribute to this observed performance degradation. The problem of high actuation voltages is addressed by the design and fabrication of driving capacitors with higher capacitive gradients while the drop in gain associated with the increased frequency spacing is a property of the concept and is dictated by the mass ratio.

CONCLUSIONS

Even though the 3-DOF gyroscope was shown to be robust to parameter variations, the 2-DOF sense mode mechanical design has drawbacks when its operational frequencies are increased. Simulations of the sense mode showed that larger peak spacings were a direct result of increasing frequencies, and that this caused a drop in both sense mode amplitude and sensitivity. Smaller mass ratios can be used to maintain peak spacings at higher operational frequencies, however, this ultimately results

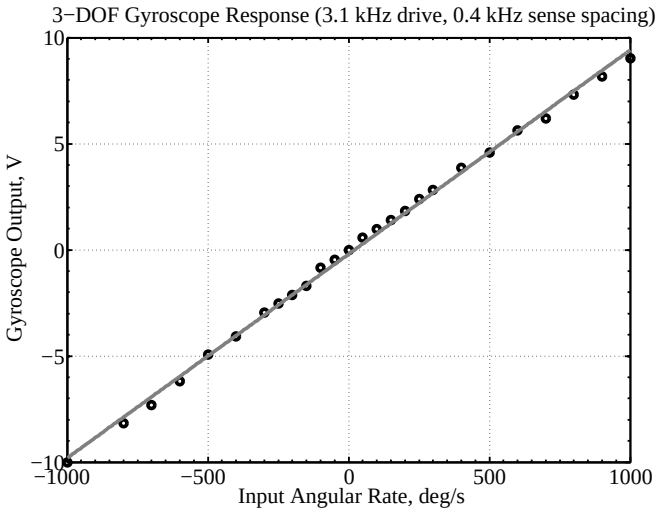

Figure 12. HIGHER FREQUENCY 3-DOF GYROSCOPE RESPONSE (3.1 KHZ DRIVE, 400 HZ PEAK SPACING)

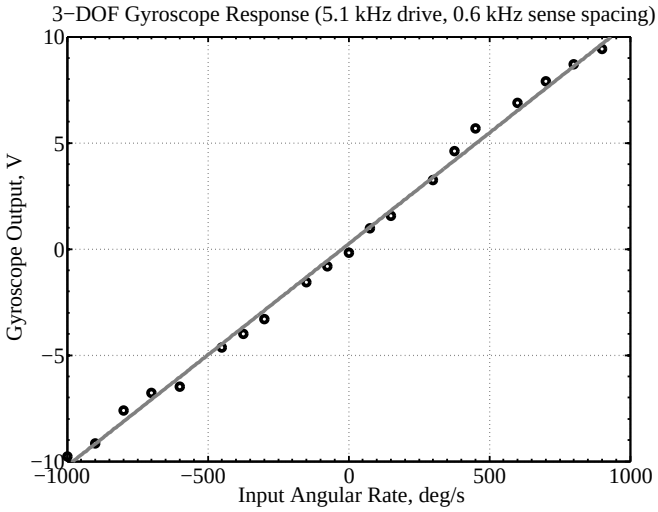

Figure 13. HIGHER FREQUENCY 3-DOF GYROSCOPE RESPONSE (5.1 KHZ DRIVE, 600 HZ PEAK SPACING)

in larger device sizes and smaller sense capacitances. Larger actuation voltages and detection biases are usually needed for operation which leads to a decrease in both the signal-to-noise ratio and sensitivity.

Despite the described challenges, the implementation of the 3-DOF concept with increased operational frequencies was shown to be feasible. Achieving even higher frequency 3-DOF gyroscopes is possible with careful mechanical design and improved fabrication resolution for increased capacitance.

ACKNOWLEDGMENT

This work was supported by BEI Technologies contract BEI-36974 and UC Discovery program ELE04-10202. We would like to acknowledge John Porter and the Carl Zeiss Center of Excellence as well as Vu Phan of the UCI Integrated Nanosystems Research Facility.

REFERENCES

[1] Shkel, A., Acar, C., and Painter, C., 2005. "Two types of micromachined vibratory gyroscopes". *IEEE Sensors Conference 2005, Irvine, California, USA*, pp. 531–536.

[2] Geen, J. A., Sherman, S. J., Chang, J. F., and Lewis, S. R., 2002. "Single-chip surface-micromachined integrated gyroscope with 50 deg/hour root allan variance". *IEEE International Solid-State Circuits Conference. Digest of Technical Papers,* **2**, pp. 346–539.

[3] Acar, C., Shkel, A. M., Costlow, L., and Madni, A. M., 2005. "Inherently robust micromachined gyroscopes with 2-dof sense-mode oscillator". *IEEE Sensors Conference 2005, Irvine, California, USA*, pp. 664–667.

[4] Acar, C., and Shkel, A. M., 2006. "Inherently robust micromachined gyroscopes with 2-dof sense-mode oscillator". *IEEE Journal of Microelectromechanical Systems,* **15**(2), pp. 380–387.

[5] Acar, C., Painter, C. C., Schofield, A. R., and Shkel, A. M., 2005. "Robust micromachined gyroscopes for automotive applications". *NSTI Nanotech 2005 Technical Proceedings*, pp. 375–378.

[6] Tang, W. C., Nguyen, T.-C. H., and Howe, R. T., 1989. "Laterally driven polysilicon resonant microstructures". *Proceedings: IEEE Micro Electro Mechanical Systems. An investigation of Micro Structures, Sensors, Actuators, Machines and Robots*, pp. 53–59.